Human vestibular schwannoma reduces density of auditory nerve fibers in the osseous spiral lamina

Eggink, M.C.; Frijns, J.H.M.; Sagers, J.E.; O'Malley, J.T.; Liberman, M.C.; Stankovic, K.M.

Hearing Research 418 (2022) 108458

Contents lists available at ScienceDirect

Hearing Research

journal homepage: www.elsevier.com/locate/heares

Human vestibular schwannoma reduces density of auditory nerve fibers in the osseous spiral lamina

Maura C. Eggink[a,b,c,d], Johan H.M. Frijns[c,e], Jessica E. Sagers[b], Jennifer T. O'Malley[b], M. Charles Liberman[a,b], Konstantina M. Stankovic[a,b,f,*]

[a] Department of Otolaryngology - Head and Neck Surgery, Harvard Medical School, Boston, MA, USA
[b] Eaton Peabody Laboratories and Department of Otolaryngology - Head and Neck Surgery, Massachusetts Eye and Ear, Boston, MA, USA
[c] Department of Otorhinolaryngology, Leiden University Medical Center, Leiden, the Netherlands
[d] Department of Otorhinolaryngology, Amsterdam UMC, location Academic Medical Center, University of Amsterdam, the Netherlands
[e] The Leiden Institute for Brain and Cognition, Leiden, the Netherlands
[f] Department of Otolaryngology, Head and Neck Surgery, Stanford University School of Medicine, Stanford, CA, USA

ARTICLE INFO

Article history:
Received 22 September 2021
Accepted 5 February 2022
Available online 7 February 2022

Keywords:
Vestibular schwannoma
Auditory nerve fiber density
Osseous spiral lamina
Hearing loss
Cellmask®
Human temporal bones

ABSTRACT

Hearing loss in patients with vestibular schwannoma (VS) is commonly attributed to mechanical compression of the auditory nerve, though recent studies suggest that this retrocochlear pathology may be augmented by cochlear damage. Although VS-associated loss of inner hair cells, outer hair cells, and spiral ganglion cells has been reported, it is unclear to what extent auditory-nerve peripheral axons are damaged in VS patients. Understanding the degree of damage VSs cause to auditory nerve fibers (ANFs) is important for accurately modeling clinical outcomes of cochlear implantation, which is a therapeutic option to rehabilitate hearing in VS-affected ears. A retrospective analysis of human temporal-bone histopathology was performed on archival specimens from the Massachusetts Eye and Ear collection. Seven patients met our inclusion criteria based on the presence of sporadic, unilateral, untreated VS. Tangential sections of five cochlear regions were stained with hematoxylin and eosin, and adjacent sections were stained to visualize myelinated ANFs and efferent fibers. Following confocal microscopy, peripheral axons of ANFs within the osseous spiral lamina were quantified manually, where feasible, and with a "pixel counting" method, applicable to all sections. ANF density was substantially reduced on the VS side compared to the unaffected contralateral side. In the upper basal turn, a significant difference between the VS side and unaffected contralateral side was found using both counting methods, corresponding to the region tuned to 2000 Hz. Even spiral ganglion cells (SGCs) contralateral to VS were affected by the tumor as the majority of contralateral SGC counts were below average for age. This observation provides histological insight into the clinical observation that unilateral vestibular schwannomas pose a long-term risk of progression of hearing loss in the contralateral ear as well. Our pixel counting method for ANF quantification in the osseous spiral lamina is applicable to other pathologies involving sensorineural hearing loss. Future research is needed to classify ANFs into morphological categories, accurately predict their electrical properties, and use this knowledge to inform optimal cochlear implant programming strategies.

VS	vestibular schwannoma
SNHL	sensorineural hearing loss, cochlear implant: CI
ABR	auditory brainstem response
IAC	internal auditory canal
DPOAEs	distortion product otoacoustic emissions
IHC	inner hair cell
OHC	outer hair cell
ANFs	auditory nerve fibers
SGCs	spiral ganglion cells
OSL	osseous spiral lamina
H&E	hematoxylin and eosin
ChAT	choline acetyltransferase

1. Introduction

Vestibular schwannoma (VS), the most common neoplasm of the cerebellopontine angle, is a non-malignant tumor that arises from Schwann cells of the vestibular nerve and presents with sensorineural hearing loss (SNHL) in 95% of patients (Dilwali et al.,

* Corresponding author at: Department of Otolaryngology, Head and Neck Surgery, Stanford University School of Medicine, Stanford, CA 94305, USA.
E-mail address: kstankovic@stanford.edu (K.M. Stankovic).

https://doi.org/10.1016/j.heares.2022.108458
0378-5955/

2015; Johnson, 1977). Mechanisms of VS-induced SNHL are multifactorial and include both retrocochlear and cochlear mechanisms (Thakur et al., 2012). Physiologic evidence for retrocochlear mechanisms, such as mechanical compression of the cochlear nerve in the internal auditory canal, includes delayed auditory brainstem response (ABR) waves and decreased ABR amplitudes (Bozorg Grayeli et al., 2008; Thomsen et al., 1978). Physiological evidence for cochlear mechanisms underlying VS-associated SNHL include decreased distortion product otoacoustic emissions (DPOAEs) in patients with mild SNHL (Gouveris et al., 2007), suggesting that outer hair cell (OHC) dysfunction could be a primary cochlear event. Studies of human VS secretions applied to murine cochlear explants indicate that VS-secreted soluble molecules (Dilwali et al., 2015, 2013) and extracellular vesicles (Soares et al., 2016) derived from VSs associated with poor hearing can cause direct cochlear damage. A clinical study of long-term bilateral hearing outcomes in patients with unilateral VS found a risk of progression to moderate hearing loss in the contralateral ear as well, also suggesting a role of tumor-secreted factors and/or immune mechanisms involved in VS-associated hearing loss (Early et al., 2020). Histopathologic examinations of human temporal bones with VS provides evidence for cochlear pathology, characterized by loss of hair cells and spiral ganglion neurons, strial atrophy, and proteinaceous precipitate in the inner ear (Mahmud et al., 2003; Roosli et al., 2012a), as well as retrocochlear pathology, characterized by atrophy of central axons of the auditory nerve within the internal auditory canal (De Moura, 1967; Eckermeier et al., 1979; Johnsson et al., 1984).

The density of auditory nerve fibers (ANFs) within the osseous spiral lamina (OSL), however, has not been studied quantitatively in VS patients. Spiral ganglion cells (SGCs), the cell bodies of ANFs, and their central axons can survive months to years after degeneration of peripheral axons, so counting only SGCs can underestimate actual neuronal damage (Felix et al., 2002; Kujawa and Liberman, 2009). Moreover, SGCs and central axons will not contribute to hearing if peripheral axons are absent. Information regarding ANF status and integrity can help support mechanistic theories for VS-induced SNHL and inform predictions for auditory outcomes in VS patients undergoing cochlear implantation.

Cochlear implants (CIs) are devices that electrically stimulate cochlear neurons, including ANFs within the OSL, and thereby restore hearing. CIs are becoming an increasingly valuable therapeutic option for patients with VS, especially when the VS develops in their only hearing ear (Lassaletta et al., 2016; Lloyd et al., 2014; Mukherjee et al., 2013). Ipsilateral cochlear implantation in VS patients with small and stable tumors and/or following VS resection or radiotherapy, has been shown to provide variable benefit, leading in some patients to improvement in open-set speech perception. Apart from the post-operative status of the cochlear nerve, other histologic parameters that underlie CI outcome variability are not well understood.

Prior methods used for ANF quantification have significant limitations. For example, electron microscopy is often necessary to achieve a high enough magnification to quantify individual ANFs (Arnesen and Osen, 1978; Spoendlin, 1972; Spoendlin and Schrott, 1989; Waaijer et al., 2013), and neither ultra-thin sectioning nor specialized microdissection techniques are amenable to use in archival human temporal bone specimens (Felder and Schrott-Fischer, 1995). Osmication of human temporal bones is also not feasible in archival specimens, as this process must be performed shortly after death (Spoendlin and Schrott, 1989).

Here we build on a recently published methodology for quantification of ANF density in the OSL of archival human temporal bones based on immunohistochemical staining of de-celloidinized cochlear sections (Wu et al., 2020), by automating the analysis with a pixel-counting approach. In prior cochlear studies, pixel counting after image thresholding has been used to quantify both efferent and afferent innervation (Irving et al., 2011; Wise et al., 2011). Our pixel counting method specifically targets myelinated type-I afferent axons and has been validated against manual ANF counts. This study provides histologic insight into the neural correlates of VS-induced hearing loss and may inform future improvements in cochlear implant programming strategies for VS patients. This new ANF counting method could also be employed to analyze anatomical substrates of other sensorineural pathologies.

2. Materials and methods

2.1. Study design and subjects

A search of the archival collection of human temporal bones at Massachusetts Eye and Ear was performed, following protocols approved by the affiliated Human Studies Committee and in accordance with the Helsinki Declaration. Patients included in the National Temporal Bone Registry provided informed consent prior to death. Patients with sporadic, unilateral, untreated, occult or symptomatic VS were included. Patients with neurofibromatosis type 2 (NF2) or confounding middle- or inner-ear pathologies were excluded (Supplementary Fig. 1). Key clinicopathologic characteristics were recorded for each patient, such as gender, age, presence of a symptomatic or occult tumor, and post-mortem time, as summarized in Table 1. Audiometric data (pure tone average of thresholds at 500, 1000 and 2000 Hz, and speech discrimination scores) were collected when available. Tumor nerve of origin (superior vestibular nerve, inferior vestibular nerve, and vestibular nerve trunk) was recorded. The maximal extent of the tumor in the x and y plane was measured in mm. Tumor thickness in the z plane was determined by counting the number of 20 μm-thick sections spanned by the tumor. Tumor volume was calculated in mm^3, assuming an elliptical tumor shape. Minimal distance from the tumor to the base of the modiolus was measured.

Human cochlear cross-sections were studied to quantify changes in density of ANFs in the OSL of patients with VS compared to the unaffected contralateral side. Selected sections were stained via protocols described below and images obtained using confocal microscopy. Two methods were applied for assessment of ANF density in the OSL: manual counting of individual ANFs ($n = 5$) and automatic quantification of saturated pixels in all the manual-count cases, plus two others where manual counts were ambiguous ($n = 7$).

2.2. Tissue preparation and immunohistochemistry

Human temporal bones were previously harvested at autopsy, fixed in formalin or Heidenhain Susa, decalcified in trichloracetic acid or ethylenediaminetetraacetate, embedded in celloidin, and serially horizontally sectioned at 20 μm; every tenth section was stained using hematoxylin and eosin (H&E), as is standard for light microscopic examination of human temporal bones (Schuknecht, 2010). Tangential cuts corresponding to five cochlear regions (1, lower basal turn; 2, upper basal turn; 3, lower middle turn; 4, upper middle turn; and 5, apex) were identified from both ears, i.e. ipsilateral and contralateral to the VS (Fig. 1A). The tangential sections selected for study in each half turn were those in which Reissner's membrane joins the limbus (Fig. 1B, Supplementary Fig. 2). At this radial position in the OSL, peripheral axons of ANFs are myelinated.

To highlight efferent axons from the olivocochlear bundle (Schrott-Fischer et al., 2007), celloidin was removed using methanol saturated with sodium hydroxide as previously described (O'Malley et al., 2009). Sections were exposed to blocking buffer (PBS with 5% normal horse serum and 0.3% Triton X-100) for 1 h at

Table 1
Clinicopathologic characteristics (n=7)

	Patient		Tumor		Audiology						Preservation
	Gender	Age (yrs)	Nerve of origin	S/O	Tumor volume (mm3)	Distance tumor – modiolus (mm)	AC (dB)	BC (dB)	SD (%)	Time before death (yrs)	Post-mortem time (h)
1	F	74	IV	O	0.5	1.7	*71.7*	*37.5*	*100*	15	9
2	M	84	SV	O	6.2	2.6	80	43.8	56	1	4.5
3	M	49	IV	O	25.3	1.5	*NA*	*NA*	*NA*	NA	22
4	M	81	SV	S	623.1	3.2	*NA*	*NA*	*NA*	NA	11
5	F	91	IV	S	932.6	5.2	*112.5*	*>120*	-	15	13
6	M	75	VN	S	1508.0	0.4	*44.2*	-	*40*	16	27
7	F	100	VN	S	2856.0	7.6	100	47.5	0	1	28

Nerve of origin – SV: superior vestibular nerve, IV: inferior vestibular nerve, VN: vestibular nerve trunk. S/O – S: symptomatic, O: occult. Audiology – AC: ipsilateral air conduction thresholds, italic values indicate thresholds obtained at >1 year before death, BC: ipsilateral bone conduction thresholds, italic values indicate thresholds obtained at >1 year before death, SD: ipsilateral speech discrimination scores, italic values indicate thresholds obtained at >1 year before death. NA: not available.

room temperature and treated overnight with goat anti-ChAT (anti-Choline Acetyltransferase) antibody (Millipore #144P) at 1:1000 dilution in 1% normal horse serum and 0.3% Triton X-100. Two consecutive applications of secondary antibodies were performed: chicken-anti-goat-AF488 (Thermo Fisher #A21467) and goat-anti-chicken-AF488 (Thermo Fisher #A11039) for an hour. To visualize myelinated ANFs, a membrane stain, CellMask ® Orange (Invitrogen #C10045), was applied at 1:2000 dilution in PBS and 0.3% Triton X-100 for 5 min. Sections were mounted in Vectashield, coverslipped, and sealed with clear nail polish.

2.3. Quantification of auditory nerve fiber density

Images of the stained sections were acquired using a Leica SP8 confocal microscope with 63x glycerol objective (N.A. 1.3). For each section, a z-stack was acquired (0.33 µm spacing) that spanned at least 1.66 µm of the 20 µm section thickness, with an average z-stack of 13.67 µm. Laser power and detector gain were adjusted to saturate the CellMask® signal in myelin sheaths, while minimizing background intensity. Scans were randomized and quantified blind to patient demographics and VS characteristics, including side. Where the quality of the staining and fiber morphology allowed for individual identification of ANFs, manual counting was performed and repeated three times within the middle 500 μm of the OSL cross-section, using the z-slice with the highest resolution (manual counting method). This method could not be applied on slides from two patients (Patient 1 and Patient 3), who were consequently excluded from manual quantification (Supplementary Fig. 1). For the pixel counting method, automatic quantification of the sections was performed using the Color Pixel Counter Plugin, developed for ImageJ (Pichette, 2010). The Color Pixel Counter Plugin counts the number of pixels of a chosen color in an image or selection of an image. A rectangular selection tool of 500 µm was used to count pixels of the stained nerve fibers within 500 µm of the osseous spiral lamina. All images were thresholded to a minimal intensity value in order to exclusively count myelinated nerve fibers stained bright red in the CellMask® channel and eliminate background noise from the quantification. This method was applied to slides from all seven patients (Supplementary Fig. 1).

2.4. Quantification of SGCs

SGC counts were conducted as described previously (Makary et al., 2011). All SGCs in which a nucleus was visible were manually counted in every tenth H&E-stained section of each cochlear turn. Total neuronal counts for each cochlea were then estimated by multiplying SGC counts by 10 to account for intervening sections, and by 0.91 to correct for dual-counting of nuclei spanning section boundaries, in accordance with the most recent recommendations (Robert and Linthicum, 2016).

2.5. Data analysis

Statistical analyses were performed using the IBM Statistical Package for Social Science (SPSS) version 24. Quantification methods for the density of ANFs in the OSL were validated using a Bland-Altman plot and a linear regression analysis. The reproducibility of manual counts in comparison to pixel counts was confirmed by calculating the intraclass correlation coefficient (0.997; single measures, one-way random model) and via a Bland-Altman plot, in which 88% of paired measurements fell within the limits of agreement. A Shapiro-Wilk test was performed to analyze the distribution of data produced by both methods. Pairwise comparisons of ANF densities ipsilateral and contralateral to the VS and of densities between cochlear regions were completed using a Wilcoxon signed-rank test. A two-way repeated measurements ANOVA using tumor-side and the five cochlear regions as independent variables (sphericity assumed under Mauchly's test of sphericity yielded a $p > 0.05$) was performed to analyze any interactions between main effects. ANF density was correlated with clinicopathologic characteristics: continuous variables were correlated with ANF densities using Spearman's correlation; categorical variables were tested with a Mann-Whitney U test; more than two categorical variables were tested with the Kruskal-Wallis test. Missing data concerning patient characteristics led to the exclusion of some patients from sub analyses dependent on those data. *P*-values <0.05 were considered significant. Where applicable, two-sided *p*-values were used.

3. Results

3.1. Patient selection

Twenty patients with unilateral, sporadic, and untreated VS met our diagnostic criteria (Supplementary Fig. 1). Four patients with intralabyrinthine schwannomas were excluded to rule out pathology caused by direct damage to ANFs. Patients with other confounding pathologies that could damage the inner ear were also excluded, such as post-meningitic ossification of the cochlea, sensorineural hearing loss following a stapedotomy, and an arachnoid cyst within the internal auditory canal with compression of the facial, cochlear and vestibular nerves. Patients with no contralateral sections available or no unstained sections available for immunostaining were also excluded. The final study group consisted of 7 patients (4 males, 3 females) with an average age of 79.1 years (range, 49–100). In accordance with previous reports, VSs

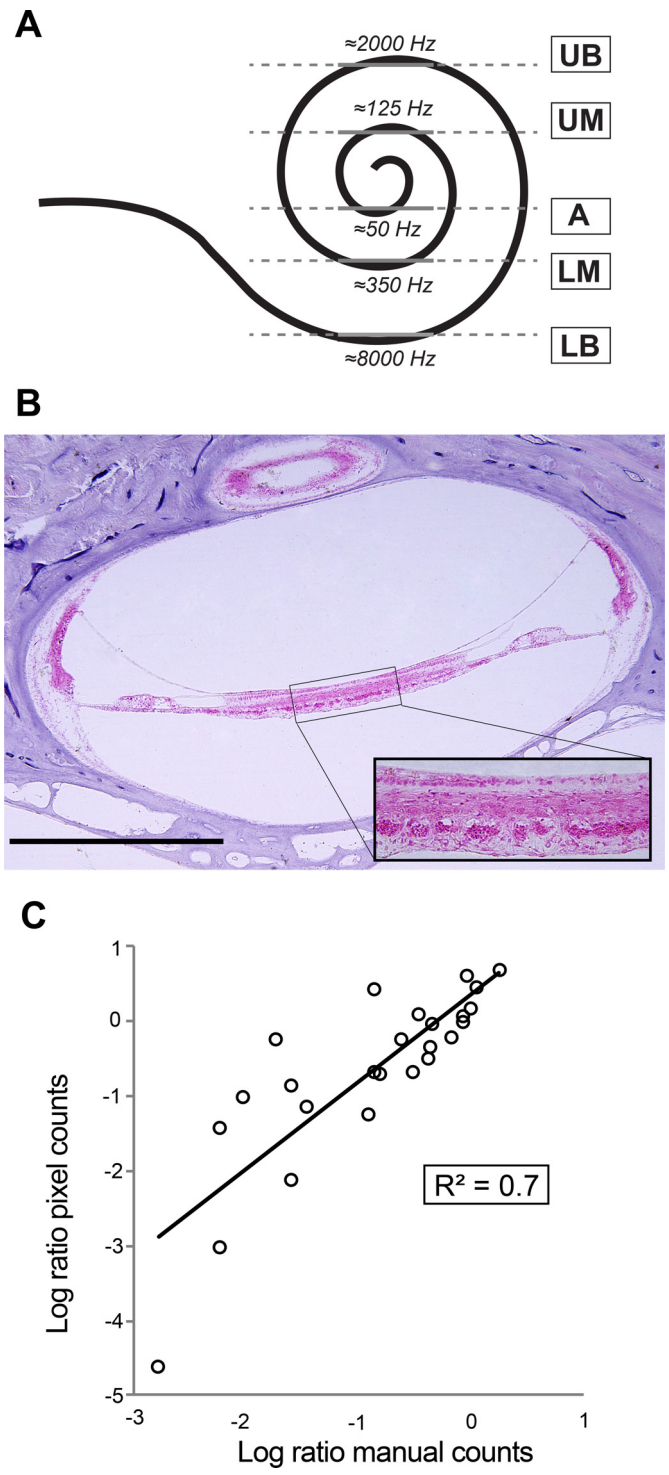

Fig. 1. Quantification of human auditory nerve fibers in tangential sections through the osseous spiral lamina. **1A**. Cochlear spiral illustrating the location of the five tangential sections studied (LB: lower basal turn; UB: upper basal turn; LM: lower middle turn; UM: upper middle turn; A: apex) and their corresponding frequencies, as estimated using standard cochlear reconstruction techniques and a cochlear map for human (Greenwood, 1990; Stakhovskaya et al., 2007) with parameters modified to yield extreme values of 120 Hz (apical tip) and 20,000 Hz (basal tip). **1B** Light micrograph of a contralateral tangential section of the upper middle turn (corresponding to segment UM in Fig. 1A) of patient 4, stained with hematoxylin and eosin; rectangular zoomed inset of osseous spiral lamina. Scale bar: 1 mm. **1C**. Scatterplot comparing the manual and pixel counting methods. Data from both methods expressed as a ratio of ipsilateral and contralateral counts, log-transformed. Each circle represents a different quantified section (5 patients, 5 slides per patient), line indicates a linear regression fit. R^2: coefficient of determination.

arose with similar frequency on the superior vestibular and inferior vestibular nerve in our patient group (Roosli et al., 2012b).

3.2. Method validation

Assessment of ANF density in the OSL was performed using two methods. Both methods relied on the staining of myelin sheaths with CellMask® membrane stain. Coupling the CellMask® with an immunostain for a cholinergic marker of efferent fibers from the olivocochlear bundle (Moore et al., 1999) we observed that, within the portions of the OSL we examined (i.e. directly under the limbus), these efferent fibers were never myelinated. Furthermore, since the afferent (sensory) fibers innervating the outer hair cells are unmyelinated throughout their course (Kiang et al., 1982), our CellMask® counts in the OSL are exclusively counting the myelinated peripheral axons of the Type I spiral ganglion cells innervating inner hair cells.

Where feasible, ANFs in the OSL were manually counted ($n = 5$ patients). Reproducibility within manual counts was validated via intraclass correlation coefficient as described above. An additional sensitivity analysis was completed by removing the lowest counts ($\leq$ 7 fibers), which did not influence the correlation. Secondly, pixel counting ($n = 7$ patients) was performed via automatic quantification of the number of CellMask® pixels (see Methods). In sum, ANF density for each patient was estimated based on 10 sections analyzed with both the pixel counting method and, whenever possible, manual counts. An equal number of sections ipsilateral and contralateral to the VS were analyzed for each patient.

To compare our pixel counting method with manual ANF counts, a Bland-Altman plot was made to express the ratios between ANF counts in the OSL ipsilateral and contralateral to the VS, as described above. A scatterplot comparing the two methods was plotted on a logarithmic scale and fitted with a linear regression line confirming this agreement ($R^2 = 0.7$, Fig. 1C), denoting that 70% of the variance in manual counts can be accounted for with pixel counts. In some cases, manual counts were too difficult, because the myelin sheaths appeared discontinuous and patchy (e.g. Patients 1 and 3, Supplementary Fig. 3), and it was difficult to unambiguously cluster the patches of signal into discrete rings.

3.3. Assessment of ANF density in the OSL

Comparison of CellMask® staining in the ipsilateral vs contralateral ear reveals an obvious reduction in the density of auditory-nerve peripheral axons ipsilateral to VS in the upper basal turn of all 7 patients (Fig. 2A and B, Supplementary Fig. 3). This visual impression is supported by quantitative measurements using manual counts ($p = 0.006$, Wilcoxon signed-rank test; Figs. 2C and 3A) and automated pixel counts ($p = 0.013$, Wilcoxon signed-rank test; Fig. 2D).

A significant interaction between ear and cochlear region suggested that the effect of the tumor on ANF density varied by region ($p = 0.029$, manual counting; $p = 0.023$, pixel counting, two-way ANOVA). Considering each region individually, the decrease between ipsilateral and contralateral sides was significant in the upper basal turn ($p = 0.043$, Wilcoxon signed-rank test), lower middle turn ($p = 0.043$) and apex ($p = 0.043$) using manual counting, and in the upper basal turn ($p = 0.018$) using pixel counting.

Comparing SGC counts of all patients to historical controls illustrates an evident decrease of SGCs ipsilateral to the VS, and in a lesser extent contralateral to the VS (Fig. 3B and 3E). The similarity in fractional loss of SGCs and peripheral axons in each case (compare counts in Fig. 3A vs 3B, not found statistically significant using Wilcoxon signed-rank test) suggests that, in contrast to cochlear aging, the neurodegeneration in these VS cases does not

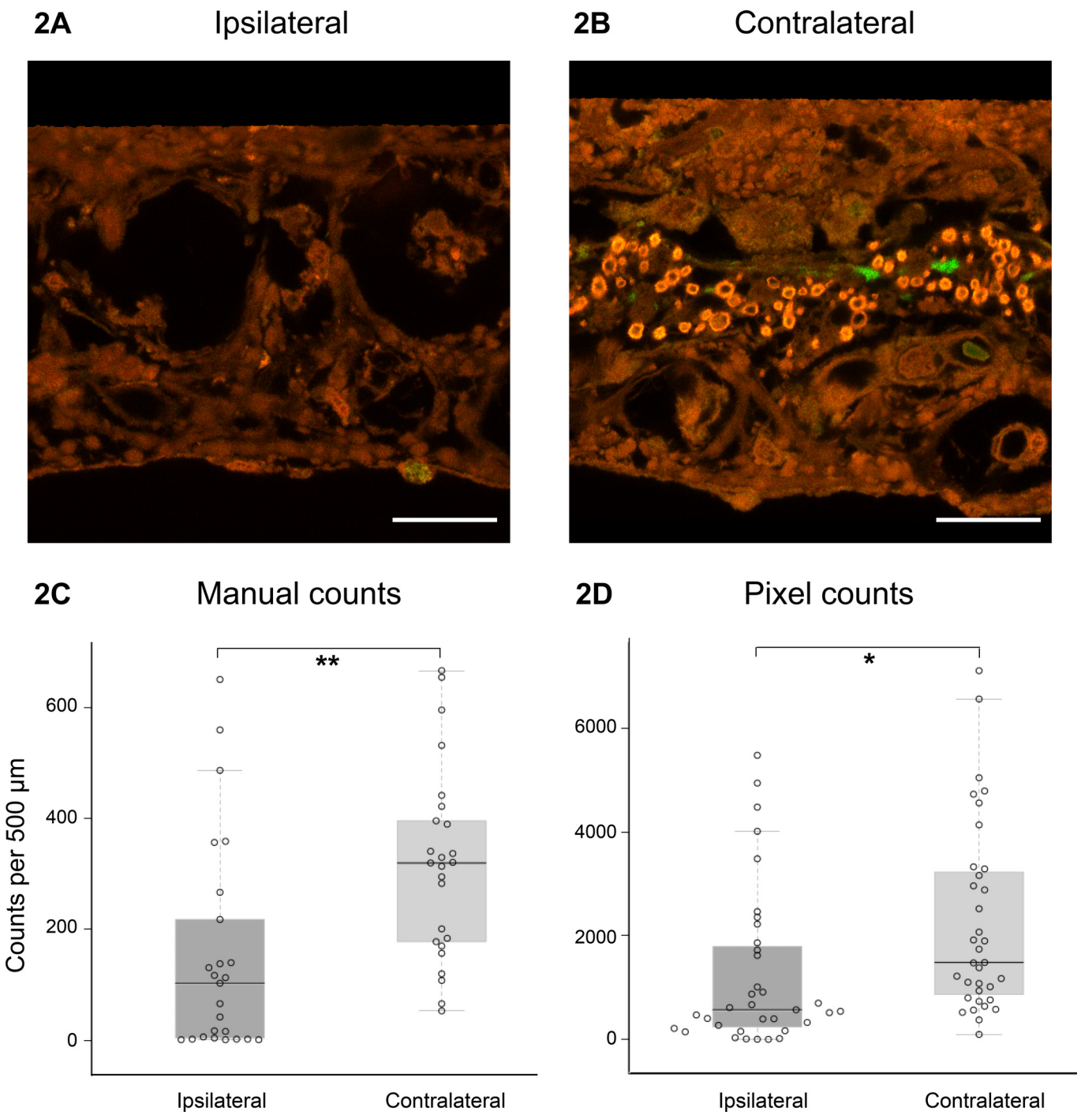

Fig. 2. Auditory nerve fiber counts are significantly decreased in the osseous spiral lamina ipsilateral to vestibular schwannoma. Confocal image of an ipsilateral (**2A**) and contralateral (**2B**) tangential section of the osseous spiral lamina in the upper basal region (section UB in Fig. 1A), of patient 5, stained with CellMask® (red) and anti-ChAT (green). Scale bar: 25 µm. **2C**. Boxplot showing auditory nerve fiber counts per 500 µm of the osseous spiral lamina, compared across all cochlear tangents for ipsilateral versus contralateral ears, obtained by the manual counting method. Center lines show medians; box limits indicate 25th and 75th percentiles; whiskers extend 1.5 times the interquartile range from 25th and 75th percentiles; individual data points plotted as open circles. $n = 5$ patients, 50 sections. $^{*}p < 0.05$, $^{**}p < 0.01$. **2D**. As 2C, obtained by the pixel counting method. $n = 7$ patients, 70 sections.

begin with the peripheral axon and thus does not leave a large population of surviving SGCs that are disconnected from their hair cell targets (Wu et al., 2019). One reason for this may be that in the four largest tumors in this study (those with the lowest number of surviving SGCs ipsilateral to tumor), there was direct invasion of the cochlear nerve by the tumor within the internal auditory canal.

3.4. Correlation of density of auditory nerve fibers in OSL with clinicopathologic characteristics

The correlations between ANF density and clinicopathologic characteristics are summarized in Table 2. Age was not correlated with ANF density in the OSL. Nerve of origin was found to have a significant influence on ANF density (manual counting, $p = 0.001$;

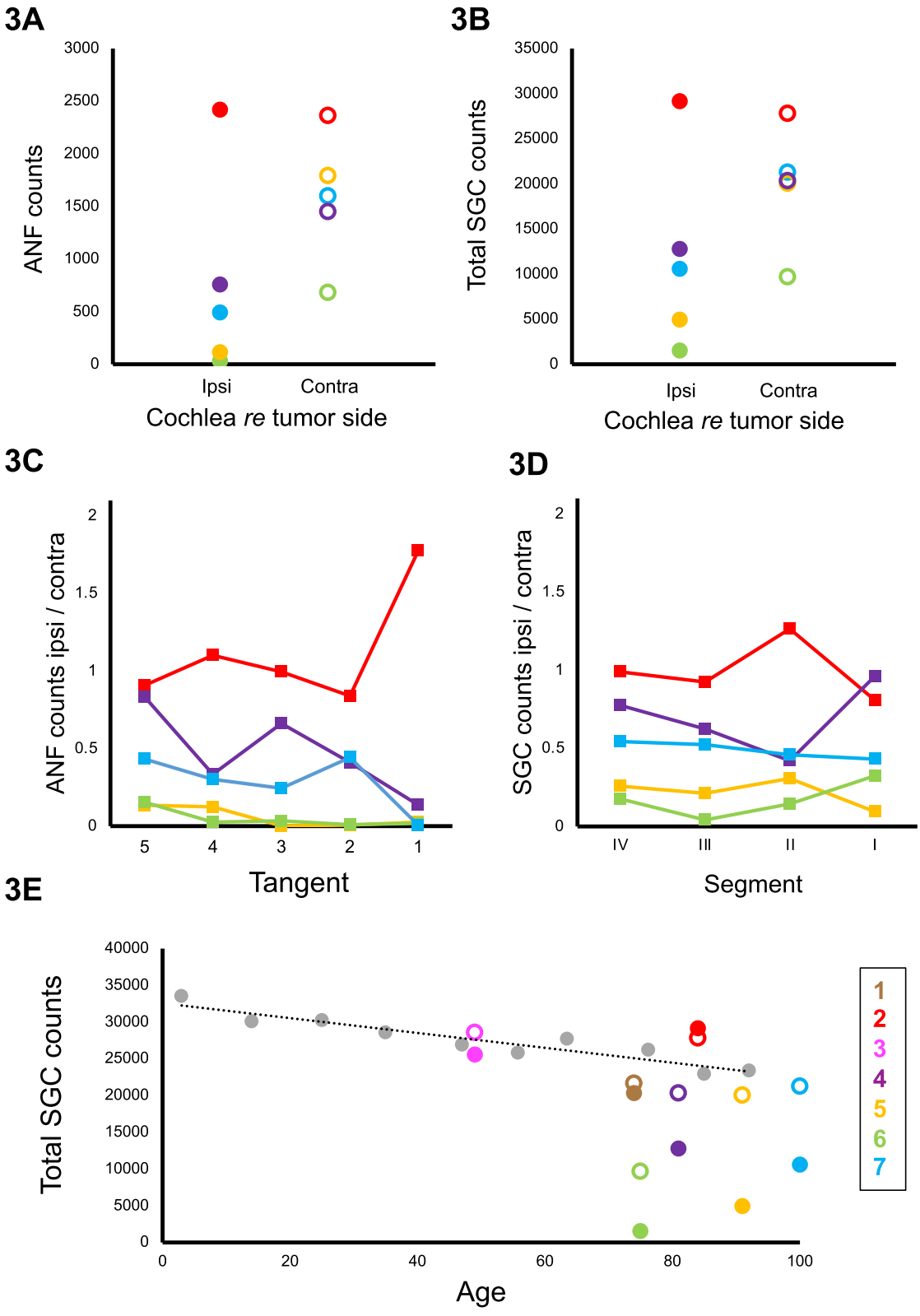

Fig. 3. Auditory-nerve fibers (ANF) and spiral ganglion cells (SGC) are evidently decreased in ears ipsilateral to vestibular schwannoma (Fig. 3A and 3B). ANF and SGC counts are affected differently by region of the cochlea (Fig. 3C and 3D). Comparison to historical controls (Makary et al., 2011) suggests both ipsilateral and contralateral fibers are affected by the tumor, as the majority of contralateral SGC counts are below the average SGC counts based on age (Fig. 3E). Tangent refers to the five tangents used to count ANFs in tangential sections, corresponding to tangential sections described in Fig. 1A (1, lower basal turn; 2, upper basal turn; 3, lower middle turn; 4, upper middle turn; and 5, apex) ascending in frequency along the *x*-axis. Segment refers to the four segments of the cochlea in which SGCs were counted (as in Merchant and Nadol, 2010), also ascending in frequency along the *x*-axis. Each patient is represented by a different color (consistent across panels; solid circles depict ipsilateral data and open circles depict contralateral data) and number (corresponding to patient numbers in Table 1).

Table 2
Correlation of density of cochlear nerve fibers with clinicopathologic characteristics

	p-value [correlation coefficient]	
	Manual counting method n=5	Pixel counting method n=7
Patient – total		
Age	*0.271*	*0.984*
Tumor – ipsilateral		
Nerve of origin	0.001	<0.001
SV - IV	0.003	<0.001
SV - VN	0.001	<0.001
IV - VN	*0.440*	*0.978*
Tumor volume	0.002 [-0.60]	0.015 [-0.41]
Distance tumor – modiolus	*0.737*	*0.955*
Audiology – ipsilateral		
AC (dB)	*0.648*	*0.347*
< 1 year of death, N=2	0.001 [-0.87]	0.001 [-0.87]
BC (dB)	0.000 [-0.86]	0.029 [-0.49]
< 1 year of death, N=2	0.001 [-0.87]	0.001 [-0.87]
SD (%)	0.031 [+0.56]	*0.500*
< 1 year of death, N=2	0.001 [+0.87]	0.001 [+0.87]

Two counting methods for the density of auditory nerve fibers are compared and contrasted. Nerve of origin – SV: superior vestibular nerve, IV: inferior vestibular nerve, VN: vestibular nerve trunk. Audiology – AC: air conduction thresholds. BC: bone conduction thresholds. SD: speech discrimination scores. Italic values indicate significance was not reached with $p<0.05$. Continuous variables were tested with a Spearman's correlation, correlation coefficient given in brackets. Categorical variables were tested with Mann-Whitney U test. More than two categorical variables were tested with the Kruskal-Wallis test.

pixel counting, $p < 0.001$, Kruskal-Wallis test). Specifically, tumors in the superior vestibular nerve were associated with significantly higher ANF densities than tumors in the vestibular nerve trunk (manual counting, $p = 0.001$; pixel counting, $p < 0.0001$; Mann-Whitney U test) or the inferior vestibular nerve (manual counting, $p = 0.003$; pixel counting, $p < 0.0001$; Mann-Whitney U test). A higher tumor volume was associated with significantly lower ANF density (manual counting, $p = 0.002$; pixel counting, $p = 0.015$, Spearman's correlation). The average distance of the tumor to the modiolus did not significantly influence ANF density (manual counting, $p = 0.737$; pixel counting, $p = 0.955$, Spearman's correlation). Consistent with VS-induced SNHL, audiometric thresholds were significantly higher and speech discrimination significantly lower in ears ipsilateral to VS than in contralateral ears. In VS-affected ears, ANF density was lower in the basal turn compared to the upper middle and apical turns, consistent with the high-frequency hearing loss often observed in VS patients (Thakur et al., 2012).

4. Discussion

To our knowledge, this is the first study to quantify decreased ANF density in the OSL ipsilateral to VS. Our finding that lower ANF densities in the OSL are observed when VSs arise from the inferior rather than the superior branch of the vestibular nerve may be explained by the proximity of the inferior branch to the cochlear nerve in the internal auditory canal. A tumor arising from the inferior nerve may more easily exert direct pressure on the cochlear nerve, compromise blood flow, or cause damage through extracellular vesicles and soluble molecules (Dilwali et al., 2013; Jacob et al., 2007; Soares et al., 2016).

Our study provides the first histological insight into the clinical observation that VS-induced SNHL typically produces the largest initial increase in audiometric thresholds around 3000 Hz (Saliba et al., 2009). Specifically, when we define loss as the ratio between ipsi- and contralateral ear, we found the greatest loss of ANFs in the upper basal turn, corresponding to a frequency of roughly 2000 Hz (Fig. 1A) (Schuknecht, 2010; Stakhovskaya et al., 2007). Although scattered loss of ANFs does not elevate audiometric thresholds, when losses exceed 80%, as they do in several of the cases studies here, that loss does begin to manifest in threshold elevations (Lobarinas et al., 2013).

Our study also suggests VS can lead to a greater scope of damage than currently recognized. There could be a systemic effect of VS as our comparison to historical controls (Makary et al., 2011) suggests both ipsilateral and contralateral SGCs are affected by the tumor: the majority of contralateral SGC counts are below the average SGC counts based on age (Fig. 3E). This histopathological finding is in line with our recent clinical study of long-term bilateral hearing outcomes in hundreds of patients with unilateral VS, which found a risk of progression to moderate hearing loss in the contralateral ear as well (Early et al., 2020). Taken together, these studies suggest a role of VS-secreted ototoxic factors or immune mechanisms involved in VS-associated hearing loss. Regarding the latter, systemic immunosuppression is known to be a hallmark feature of intracranial cancer and other intracranial pathologies such as stroke and traumatic brain injury (Chongsathidkiet et al., 2018; Meisel et al., 2005). Whether similar systemic immunosuppression exists in VS remains to be determined.

Here, we present a reliable, efficient pixel-counting quantification method for assessment of unilateral neural degeneration in archived temporal bone sections as an alternative to manual quantification of ANFs. By using contralateral ears as controls, we eliminate important confounding variables such as age, genetic profile, postmortem time, and shelf time.

Our pixel counting method allowed for the analysis of ANFs in temporal bone sections from an additional two patients for whom manual counts were too ambiguous, due to patchy staining, and promises to optimize the usage of scarce temporal bone sections. One limitation of this method concerns axonal myelin thickness, as increases in myelin thickness or preferential degeneration of high-spontaneous-rate ANFs with large diameters could potentially lead to an overestimation of the number of ANFs still present in the OSL (Kawase and Liberman, 1992; Spoendlin and Schrott, 1989). Another challenge is posed by the phenomenon of beading, or the formation of varicose swellings within a nerve fiber due to postmortem autolysis or pathology (Gutmann and Holubar, 1950). Fur-

ther studies using electron microscopy in human temporal bone sections should be conducted to investigate the specific effects of VS on axon diameter and myelination.

Performing a histologic study on archival human temporal bone sections poses clear methodologic challenges. Despite the scarcity of human temporal bone with VS in archives, it would be ideal to repeat this study in a larger cohort, possibly from bones housed in multiple centers, to strengthen these conclusions and analyze possible confounding variables. Importantly, we focused on quantifying only myelinated, type-I afferent fibers, which represent 95% of sensory fibers in the cochlea (Spoendlin, 1985). Though unmyelinated type II afferent nerve fibers were not included in our analyses, it remains an open question as to whether these fibers contribute to CI-relevant clinical outcomes.

Our findings may be relevant to the prediction of clinical outcomes following cochlear implantation in VS patients with small and stable tumors or with intact cochlear nerves following resection or radiotherapy. Although it is likely that spiral ganglion cells remain electrically excitable whether or not the peripheral axon survives, the peripheral axons of the auditory nerve may be preferentially targeted by laterally placed electrodes. Further analysis of the morphology of ANFs in this region in terms of diameter and myelin thickness may elucidate the electrical properties of these fibers and contribute to the optimization of CI programming strategies. This study lays the foundation for future research to quantify cochlear axon morphology in larger VS patient cohorts and in patients with other inner ear pathologies.

5. Conclusion

This study represents the first quantitative analysis of auditory nerve peripheral axons in patients with VS. Our data demonstrate a clear decrease in ANF density in the OSL ipsilateral to VS, accompanied by a decrease in SGC density. A significant loss of ANFs was found in the upper basal cochlear turn using both counting methods, corresponding to a frequency of 2000 Hz. Even SGC counts contralateral to VS were reduced compared to age-based SGC counts in individuals without VS, lending mechanistic insight into the clinical observation that unilateral VS can also cause contralateral hearing loss. The pixel counting method we developed for the quantification of ANFs in the OSL is potentially applicable to other sensorineural hearing loss pathologies. Our data may provide insight into the clinical outcomes of ipsilateral cochlear implantation in VS patients. Future research is needed to analyze the electrical properties of ANFs in VS patients and use these data to optimize cochlear implant programming strategies.

Declaration of Competing Interest

The authors disclose no conflict of interest.

Source of funding

This work was supported by grants from the National Institute on Deafness and Other Communication Disorders R01DC015824 (K.M.S.), R01 DC 0188 (M.C.L.) and P50 DC015857 (M.C.L.), Nancy Sayles Day Foundation (K.M.S.), the Lauer Tinnitus Research Center (K.M.S., M.C.L) and the Bertarelli Foundation (K.M.S.).

Acknowledgments

We thank Garyfallia Pagonis for the H&E micrographs, Leslie Liberman for help with the immunohistochemistry, and Diane Jones for preparing the temporal bone sections for immunohistochemistry. We also thank Ben Pichette for the development of the Pixel Counter PlugIn for ImageJ and his help in advising us in the effective use of his tool.

Supplementary materials

Supplementary material associated with this article can be found, in the online version, at doi:10.1016/j.heares.2022.108458.

Supplementary Fig. 1: Flowchart illustrating patient selection. Peripheral auditory-nerve fibers were quantified in immunohistochemically stained cochlear sections using the manual counting method ($n = 5$) and the pixel counting method ($n = 7$). VS: vestibular schwannoma.

Supplementary Fig. 2: Schematic representing the tangential plane of section (dashed line) in the osseous spiral lamina (OSL) in a modiolar cross-section of the cochlear duct. Tangential sections are chosen to be at the radial position roughly at the intersection of Reissner's membrane (RM) and the limbus. Modified after Liberman and Kujawa, 2017.

Supplementary Fig. 3: Confocal images of tangential sections of the osseous spiral lamina in the upper basal region (corresponding to section UB in Fig. 1A) for all 7 patients (as in Table 1) stained with CellMask® (red) and anti-ChAt (green), a ipsilateral, b contralateral to vestibular schwannoma. Scale bar: 25 µm, inset: 10 × 10 µm.

References

Arnesen, A.R., Osen, K.K., 1978. The cochlear nerve in the cat: topography, cochleotopy, and fiber spectrum. J. Compart. Neurol. 178, 661–678. doi:10.1002/cne.901780405.

Bozorg Grayeli, A., Refass, A., Smail, M., Elgarem, H., Kalamarides, M., Bouccara, D., Sterkers, O., 2008. Diagnostic value of auditory brainstem responses in cerebellopontine angle tumours. Acta Oto Laryngol. 128, 1096–1100. doi:10.1080/00016480701881803.

Chongsathidkiet, P., Jackson, C., Koyama, S., Loebel, F., Cui, X., Farber, S.H., Woroniecka, K., Elsamadicy, A.A., Dechant, C.A., Kemeny, H.R., Sanchez-Perez, L., Cheema, T.A., Souders, N.C., Herndon, J.E., Coumans, J.V., Everitt, J.I., Nahed, B.V., Sampson, J.H., Gunn, M.D., Martuza, R.L., Dranoff, G., Curry, W.T., Fecci, P.E., 2018. Sequestration of T cells in bone marrow in the setting of glioblastoma and other intracranial tumors. Nat. Med. 24. doi:10.1038/s41591-018-0135-2.

De Moura, L.F., 1967. Inner ear pathology in acoustic neurinoma. Arch. Otolaryngol. 85, 125–133 (Chicago, Ill1960.

Dilwali, S., Landegger, L.D., Soares, V.Y.R., Deschler, D.G., Stankovic, K.M., 2015. Secreted factors from human vestibular schwannomas can cause cochlear damage. Nat. Publ. Gr. 10.1038/srep18599

Dilwali, S., Lysaght, A., Roberts, D., Barker, F.G., McKenna, M.J., Stankovic, K.M., 2013. Sporadic vestibular schwannomas associated with good hearing secrete higher levels of fibroblast growth factor 2 than those associated with poor hearing irrespective of tumor size. Otol. Neurotol. 34, 748–754. doi:10.1097/MAO.0b013e31828048ec.

Early, S., Rinnooy Kan, C.E., Eggink, M., Frijns, J.H.M., Stankovic, K.M., 2020. Progression of contralateral hearing loss in patients with sporadic vestibular schwannoma. Front. Neurol. 11. doi:10.3389/fneur.2020.00796.

Eckermeier, L., Pirsig, W., Mueller, D., 1979. Histopathology of 30 non-operated acoustic schwannomas. Arch. Otorhinolaryngol. 222, 1–9.

Felder, E., Schrott-Fischer, A., 1995. Quantitative evaluation of myelinated nerve fibres and hair cells in cochleae of humans with age-related high-tone hearing loss. Hear. Res. 91, 19–32. doi:10.1016/0378-5955(95)00158-1.

Felix, H., Pollak, A., Gleeson, M., Johnsson, L.G., 2002. Degeneration pattern of human first-order cochlear neurons. Adv. Otorhinolaryngol. 59, 116–123.

Gouveris, H.T., Victor, A., Mann, W.J., 2007. Cochlear origin of early hearing loss in vestibular schwannoma. Laryngoscope 117, 680–683. doi:10.1097/MLG.0b013e31803146c5.

Greenwood, D.D., 1990. A cochlear frequency-position function for several species—29 years later. J. Acoust. Soc. Am. 87, 2592–2605. doi:10.1121/1.399052.

Gutmann, E., Holubar, J., 1950. The degeneration of peripheral nerve fibers. J. Neurol. Neurosurg. Psychiatr. 13, 89–105. doi:10.1136/JNNP.13.2.89.

Irving, S., Moore, D.R., Liberman, M.C., Sumner, C.J., 2011. Olivocochlear efferent control in sound localization and experience-dependent learning. J. Neurosci. 31. doi:10.1523/JNEUROSCI.2679-10.2011.

Jacob, A., Robinson, L.L., Bortman, J.S., Yu, L., Dodson, E.E., Welling, D.B., 2007. Nerve of origin, tumor size, hearing preservation, and facial nerve outcomes in 359 vestibular schwannoma resections at a tertiary care academic center. Laryngoscope 117, 2087–2092. doi:10.1097/MLG.0b013e3181453a07.

Johnson, E.W., 1977. Auditory test results in 500 cases of acoustic neuroma. Arch. Otolaryngol. 103, 152–158.

Johnsson, L.G., Hawkins, J.E., Rouse, R.C., 1984. Sensorineural and vascular changes in an ear with acoustic neurinoma. Am. J. Otolaryngol. Neck Med. Surg. 5, 49–59. doi:10.1016/S0196-0709(84)80020-4.

Kawase, T., Liberman, M.C., 1992. Spatial organization of the auditory nerve according to spontaneous discharge rate. J. Compart. Neurol. 319, 312–318. doi:10.1002/cne.903190210.

Kiang, N., Rho, J., Northrop, C., Liberman, M., Ryugo, D., 1982. Hair-cell innervation by spiral ganglion cells in adult cats. Science 217 (80), 175–177.
Kujawa, S.G., Liberman, M.C., 2009. Adding insult to injury: cochlear nerve degeneration after "temporary" noise-induced hearing loss. J. Neurosci. 29, 14077–14085. doi:10.1523/JNEUROSCI.2845-09.2009.
Lassaletta, L., Aristegui, M., Medina, M., Aranguez, G., Pérez-Mora, R.M., Falcioni, M., Gavilán, J., Piazza, P., Sanna, M., 2016. Ipsilateral cochlear implantation in patients with sporadic vestibular schwannoma in the only or best hearing ear and in patients with NF2. Eur. Arch. Otorhinolaryngol. 273, 27–35. doi:10.1007/s00405-014-3450-3.
Lloyd, S.K.W., Glynn, F.J., Rutherford, S.A., King, A.T., Mawman, D.J., O'Driscoll, M.P., Evans, D.G.R., Ramsden, R.T., Freeman, S.R.M., 2014. Ipsilateral cochlear implantation after cochlear nerve preserving vestibular schwannoma surgery in patients with neurofibromatosis type 2. Otol. Neurotol. Off. Publ. Am. Otol. Soc. Am. Neurotol. Soc. [and] Eur. Acad. Otol. Neurotol 35, 43–51. doi:10.1097/MAO.0000000000000185.
Lobarinas, E., Salvi, R., Ding, D., 2013. Insensitivity of the audiogram to carboplatin induced inner hair cell loss in chinchillas. Hear. Res. 302, 113–120. doi:10.1016/j.heares.2013.03.012.
Mahmud, M.R., Khan, A.M., Nadol Jr, J.B., 2003. Histopathology of the inner ear in unoperated acoustic neuroma. Ann. Otol. Rhinol. Laryngol. 112, 979–986.
Makary, C.A., Shin, J., Kujawa, S.G., Liberman, M.C., Merchant, S.N., 2011. Age-related primary cochlear neuronal degeneration in human temporal bones. JARO J. Assoc. Res. Otolaryngol. 12, 711–717. doi:10.1007/s10162-011-0283-2.
Meisel, C., Schwab, J.M., Prass, K., Meisel, A., Dirnagl, U., 2005. Central nervous system injury-induced immune deficiency syndrome. Nat. Rev. Neurosci. doi:10.1038/nrn1765.
Moore, J.K., Simmons, D.D., Guan, Y.L., 1999. The human olivocochlear system: organization and development. Audiol. Neurootol. 4, 311–325. doi:10.1159/000013855.
Mukherjee, P., Ramsden, J.D., Donnelly, N., Axon, P., Saeed, S., Fagan, P., Irving, R.M., 2013. Cochlear implants to treat deafness caused by vestibular schwannomas. Otol. Neurotol. 34, 1291–1298. doi:10.1097/MAO.0b013e31829763a7.
O'Malley, JT, Burgess, BJ, Jones, DD, Adams, JC, Merchant, SN, 2009. Techniques of celloidin removal from temporal bone sections. Ann Otol Rhinol Laryngol 118, 435–441.
Robert, M.E., Linthicum, F.H., 2016. Empirical derivation of correction factors for human spiral ganglion cell nucleus and nucleolus count units. Otolaryngol. Head Neck Surg. 154, 157–163. doi:10.1177/0194599815603964, (United States).
Roosli, C., Linthicum, F.H., Cureoglu, S., Merchant, S.N., 2012a. Dysfunction of the cochlea contributing to hearing loss in acoustic neuromas: an underappreciated entity. Otol. Neurotol. 473–480.
Roosli, C., Linthicum, F.H., Cureoglu, S., Merchant, S.N., 2012b. What is the site of origin of cochleovestibular schwannomas? Audiol. Neurotol. doi:10.1159/000331394.
Saliba, I., Martineau, G., Chagnon, M., 2009. Asymmetric hearing loss: rule 3,000 for screening vestibular schwannoma. Otol. Neurotol. Off. Publ. Am. Otol. Soc. Am. Neurotol. Soc. [and] Eur. Acad. Otol. Neurotol 30, 515–521. doi:10.1097/MAO.0b013e3181a5297a.
Schrott-Fischer, A, Kammen-Jolly, K., Scholtz, a, Rask-Andersen, H., Glueckert, R., Eybalin, M., 2007. Efferent neurotransmitters in the human cochlea and vestibule. Acta Oto Laryngol. 127, 13–19. doi:10.1080/00016480600652123.
Schuknecht, H.F., 2010. Schuknecht's Pathology of the Ear. People's Medical Publishing House, USA, Shelton.
Soares, V.Y.R., Atai, N.A., Fujita, T., Dilwali, S., Sivaraman, S., Landegger, L.D., Hochberg, F.H., Oliveira, C.A.P.C., Bahmad, F., Breakefield, X.O., Stankovic, K.M., 2016. Extracellular vesicles derived from human vestibular schwannomas associated with poor hearing damage cochlear cells. Neuro Oncol. doi:10.1093/neuonc/now099.
Spoendlin, H., 1985. Anatomy of cochlear innervation. Am. J. Otolaryngol. 6, 453–467.
Spoendlin, H., 1972. Innervation densities of the cochlea. Acta Otolaryngol. 73, 235–248. doi:10.3109/00016487209138937.
Spoendlin, H., Schrott, A., 1989. Analysis of the human auditory nerve. Hear. Res. 43, 25–38 0378-5955(89)90056-7 [pii].
Stakhovskaya, O., Sridhar, D., Bonham, B.H., Leake, P.A., 2007. Frequency map for the human cochlear spiral ganglion: implications for cochlear implants. JARO J. Assoc. Res. Otolaryngol. 8, 220–233. doi:10.1007/s10162-007-0076-9.
Thakur, J.D., Banerjee, A.D., Khan, I.S., Sonig, A., Shorter, C.D., Gardner, G.L., Nanda, A., Guthikonda, B., 2012. An update on unilateral sporadic small vestibular schwannoma. Neurosurg. Focus 33. doi:10.3171/2012.6.FOCUS12144, E1.
Thomsen, J., Terkildsen, K., Osterhammel, P., 1978. Auditory brain stem responses in patients with acoustic neuromas. Scand. Audiol. 7, 179–183.
Waaijer, L., Klis, S.F.L., Ramekers, D., Van Deurzen, M.H.W., Hendriksen, F.G.J., Grolman, W., 2013. The peripheral processes of spiral ganglion cells after intracochlear application of brain-derived neurotrophic factor in deafened guinea pigs. Otol. Neurotol. 34, 570–578. doi:10.1097/MAO.0b013e31828687b1.
Wise, A.K., Fallon, J.B., Neil, A.J., Pettingill, L.N., Geaney, M.S., Skinner, S.J., Shepherd, R.K., 2011. Combining cell-based therapies and neural prostheses to promote neural survival. Neurotherapeutics 8, 774–787. doi:10.1007/s13311-011-0070-0.
Wu, P., O'Malley, J.T., de Gruttola, V., Liberman, M.C., 2020. Age-related hearing loss is dominated by damage to inner ear sensory cells, not the cellular battery that powers them. J. Neurosci. 40. doi:10.1523/jneurosci.0937-20.2020.
Wu, P.Z., Liberman, L.D., Bennett, K., de Gruttola, V., O'Malley, J.T., Liberman, M.C., 2019. Primary neural degeneration in the human cochlea: evidence for hidden hearing loss in the aging ear. Neuroscience 407, 8–20. doi:10.1016/j.neuroscience.2018.07.053.